Elasticity and Phase Behavior of DPPC Membrane Modulated by Cholesterol, Ergosterol, and Ethanol

Kara J. Tierney,*† David E. Block,*† and Marjorie L. Longo*
*Department of Chemical Engineering and Materials Science, and †Department of Viticulture and Enology, University of California, Davis, California 95616

ABSTRACT Giant vesicles formed of 1,2-dipalmitoylphosphatidylcholine (DPPC) and sterols (cholesterol or ergosterol) in water and water/ethanol solutions have been used to examine the effect of sterol composition and ethanol concentration on the area compressibility modulus (K_a), overall mechanical behavior, vesicle morphology, and induction of lipid alkyl chain interdigitation. Our results from micropipette aspiration suggest that cholesterol and ergosterol impact the order and microstructure of the gel ($L_{\beta'}$) phase DPPC membrane. At low concentration (10–15 mol%) these sterols disrupt the long-range lateral order and fluidize the membrane ($K_a \sim 300$ mN/m). Then at 18 mol%, these sterols participate in the formation of a continuous cohesive liquid-ordered (L_o) phase with a sterol-dependent membrane density ($K_a \sim 750$ for DPPC/ergosterol and $K_a \sim 1100$ mN/m for DPPC/cholesterol). Finally at ~40 mol% both cholesterol and ergosterol impart similar condensation to the membrane ($K_a \sim 1200$ mN/m). Introduction of ethanol (5–25 vol%) results in drops in the magnitude of K_a, which can be substantial, and sometimes individual vesicles with lowered K_a reveal two slopes of tension versus apparent area strain. We postulate that this behavior represents disruption of lipid-sterol intermolecular interactions and therefore the membrane becomes interdigitation prone. We find that for DPPC vesicles with sterol concentrations of 20–25 mol%, significantly more ethanol is required to induce interdigitation compared to pure DPPC vesicles; ~7 vol% more for ergosterol and ~10 vol% more for cholesterol. For lower sterol concentrations (10–15 mol%), interdigitation is offset, but by <5 vol%. These data support the idea that ergosterol and cholesterol do enhance survivability for cells exposed to high concentrations of ethanol and provide evidence that the appearance of the interdigitated ($L_{\beta}I$) phase bilayer is a major factor in the disruption of cellular activity, which typically occurs between ~12 and ~16 vol% ethanol in yeast fermentations. We summarize our findings by producing, for the first time, "elasticity/phase diagrams" over a wide range of sterol (cholesterol and ergosterol) and ethanol concentrations.

INTRODUCTION

Sterols are essential for the organization and function of membranes in eukaryotic cells and the type of sterol present is the product of a long biochemical evolution (1,2). Our general understanding of the biophysical and physiological roles of sterols comes mainly from studies of cholesterol, the major sterol present in plasma membranes of higher eukaryotes (for reviews see Bloom et al. and others (3–7)). In fluid-phase lipids, cholesterol decreases membrane fluidity whereas in gel-phase lipids, cholesterol increases the membrane fluidity forming the so-called liquid-ordered (L_o) phase. The L_o phase is characterized by very close intermolecular spacing (i.e., a highly condensed membrane with high cohesion), a lack of long-range order (and resulting reasonable lateral fluidity), and an increased distance between lipid headgroups as cholesterol is believed to act as a spacer molecule. In heterogeneous model membranes, cholesterol tends to partition with gel-phase lipids—forming domains that are generally believed to be in the L_o phase. In living cells, these submicron-scale pools have been termed ''lipid rafts'' and experimental evidence points to their enrichment in cholesterol and long-chain saturated sphingo- and phosphatidylcholine (PC) lipids and specific proteins that are implicated in cell signaling and trafficking (for reviews see Vereb et al. and others (8,9)).

Although higher eukaryotes contain cholesterol as their major sterol component, the plasma membranes of lower eukaryotes, such as certain protozoa, yeast, and other fungi, and of insects such as *Drosophila*, contain ergosterol (1,2). The chemical structure of ergosterol differs from that of cholesterol by the presence of two additional double bonds (at positions C7 and C22) and a methyl group at C24 of the side chain (see Fig. 1). Recently, lipid rafts have been isolated from organisms that have ergosterol as their major sterol component such as the yeast *Saccharomyces cerevisiae* (10) and *Drosophila* (11). Although detailed biophysical characterization of the effect of cholesterol on model and living membranes is well documented, the effect of ergosterol on the organization, dynamics, and mechanics of membranes has not been studied in detail, especially over the relevant concentration range for organisms containing ergosterol (~10–~25 mol%) (11–15) and in comparison to cholesterol over this concentration range.

In addition to sterols, we are also interested in the biophysical and physiological effects of ethanol on lipid bilayers and mechanisms by which sterols might protect membranes from the deleterious impact of ethanol. It is now generally accepted that ethanol molecules adsorb to the polar headgroups of the membrane's lipid molecules, preferring

Submitted December 19, 2004, and accepted for publication July 1, 2005.

Address reprint requests to Marjorie L. Longo, Tel.: 530-754-6348; Fax: 530-752-1031; E-mail: mllongo@ucdavis.edu.

0006-3495/05/10/2481/13 $2.00

doi: 10.1529/biophysj.104.057943

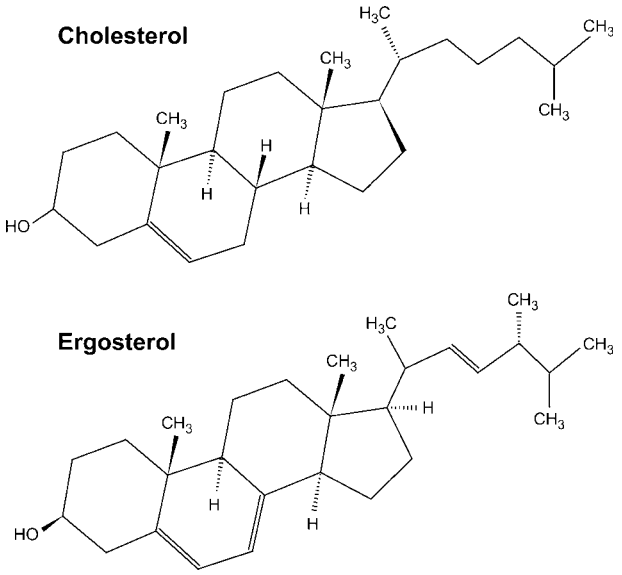

FIGURE 1 Chemical structures of the sterols used.

the region of the headgroup nearest the tails (16–22). For phosphatidylcholine lipids in the L_{β}' (gel) phase (see Table 1 for phase nomenclature), ethanol adsorption increases headgroup volume and disorders lipid chains (23). The headgroup effect appears to dominate and leads to chain tilt, and then finally complete chain interdigitation at ~12 vol% ethanol, with resulting increased headgroup motion (20,23–30). In live cells, ethanol has been observed to increase membrane fluidity (31) and induce the $L_{\beta}I$ (interdigitated gel) phase (32,33). Biologically, the substantial thickness decrease (e.g., 33%) and area expansion (e.g., 50%) that accompany the L_{β}'-$L_{\beta}I$ transition (for example, see Ly and Longo (34)) should strongly impact membrane and cellular functions.

Cholesterol appears to provide protection against the deleterious biophysical effects of small solvent molecules interacting with gel-phase lipid bilayers, in particular interdigitation induced by ethanol (25,35,36). In model membranes exposed to 12 vol% ethanol, it has been shown that the ratio of $L_{\beta}I$ phase to L_{β}' phase can be gradually decreased by increasing the membrane concentration of cholesterol, with the complete elimination of the $L_{\beta}I$ phase achieved at 20 mol% cholesterol (25). We know of no study investigating interdigitation in a wide range of ethanol and cholesterol concentrations. Therefore, it is unknown if larger concentrations of ethanol can overcome the inhibitory effect of cholesterol and by what mechanism this would occur.

Although there are a handful of studies on interdigitation in cholesterol-containing model membranes, no studies on interdigitation in ergosterol-containing model membranes exist to our knowledge. This is of particular interest in the area of ethanol production by fermenting organisms where ethanol concentrations typically reach ~14 vol% (37–40). Potentially, fermenting cells, such as yeasts, have evolved ''survival factors'' into their membrane structure, which allow the membrane to become ''tolerant'' of ethanol in its environment (37,41–43). These factors may help to protect membranes from the deleterious effects of ethanol on membrane microstructure and dynamics and include the composition of membrane lipids with regards to headgroups, chain lengths, saturation level, and sterol content. Whether the presence of ergosterol in ''normal levels'' present in yeasts (~10–25 mol%) provides a significant protective effect is an open question.

TABLE 1 Phase nomenclature

Phase	Nomenclature
Untilted liquid-ordered phase	L_o
Tilted gel phase	L_{β}'
Interdigitated gel phase	$L_{\beta}I$

In our previous work, we demonstrated that short-chain alcohols (methanol, ethanol, propanol, and butanol) can significantly decrease the elastic moduli and increase the area per molecule of fluid-phase PCs (44,45). Here, we provide the first study of the area compressibility behavior and interdigitation state of gel-phase PCs over a wide range of cholesterol and ergosterol membrane concentrations, and ethanol solution concentrations. This study covers the full physiological concentration range of sterols and the range of ethanol pertinent to fermenting organisms (and beyond). We have chosen 1,2-dipalmitoylphosphatidylcholine (DPPC) as the gel-phase lipid component. Here, as in our previous study, we utilize micropipette aspiration (MPA) of giant unilamellar vesicles (GUVs). For a general review and the theoretical framework of the technique, see Needham and Zhelev (46,47). Unlike other techniques (e.g., x-ray diffraction or neutron diffraction) that average over a large population of multilamellar vesicles, the MPA technique provides a unique opportunity to probe the structural and mechanical properties of the single bilayer of individual giant vesicles directly. MPA has been applied successfully to measure the mechanical and viscous properties of natural and synthetic systems (i.e., red blood cells (48), egg lecithin vesicle (49), diblock copolymers (50), and multicomponent lipid systems (51)). MPA has been used to observe adsorption of small molecules into the bilayer and the accompanying area expansion (e.g., the influenza hemaglutinin fusion peptide (52–54), lysolipid (55), and low molecular weight polymer surfactant (56)). In addition to MPA, we visually inspected the vesicles to assist in identification of fluidity and the presence of the $L_{\beta}I$ phase in the membranes. We discuss our results with respect to: concentration-dependent changes in L_{β}' and L_o domain organization and intermolecular distance; the differential roles and physiological concentrations of ergosterol versus cholesterol in plasma membranes of eukaryotic organisms; inhibition of interdigitation by sterols (and suggest a mechanism for ethanol to overcome the inhibitory effect); and the potential that ergosterol provides significant protection against interdigitation in fermenting organisms. Moreover, we create ''elasticity diagrams'' and overlay suggested

''phase diagrams'' based on discontinuities in area compressibility modulus, general mechanical behavior (liquid versus gel), and visual appearance of vesicles.

MATERIALS AND METHODS

Materials

DPPC and cholesterol (>98% purity) were obtained from Avanti Polar Lipids (Alabaster, AL). Ergosterol (98% purity) and high-performance liquid chromatography grade chloroform and methanol were purchased from Fisher Scientific (Fairlawn, NJ). Glucose and sucrose of ultragrade were obtained from Sigma-Aldrich (St. Louis, MO). Bovine serum albumin (fraction V, low heavy metals) was purchased from Calbiochem (San Diego, CA). Ethanol (200 proof) was acquired from Gold Shield Chemical (Hayward, CA). Deionized water was purified to a resistivity of 18.1 MΩ-cm by a Barnstead Nanopure water system (Dubuque, IA).

Sample preparation

Preparation of giant unilamellar vesicles

Giant unilamellar vesicles were produced using the electroformation method (57). Stock solutions of all lipids were diluted to 0.5 mg/mL in a mixed solvent of 2:1 (vol/vol) chloroform to methanol. These new solutions were combined in various mol/mol ratios, depending on the vesicle composition needed for experimentation. Using a syringe, 50 μL of the appropriately combined solution was coated evenly onto two parallel platinum wires, separated by 3 mm. The wires were housed in an open rectangular center of a Teflon block. The solvent was evaporated using a light stream of nitrogen gas. The remaining solvent was removed by placing the wires under vacuum for at least 2 h. The open center of the block was sealed into a chamber by two SurfaSil (Pierce Biotechnology, Rockford, IL) coated glass coverslips using vacuum grease. The chamber was filled with a 100 mM sucrose aqueous solution that had been preheated to ~50°C, i.e., above the 41°C phase transition temperature of DPPC (58). The chamber was then submerged in a preheated sucrose solution and placed in a ~50°C oven. A series of sine waves (3 volts peak to peak) were applied across the wires at 10 Hz for 30 min, 3 Hz for 15 min, 1 Hz for 7 min, and 0.5 Hz for 7 min using a function generator (Tenma, Centerville, OH). The temperature of the solution in which the chamber was submerged was carefully monitored throughout the electroformation process to make sure it did not fall below 49°C. When finished, GUVs ranging in size from 10–60 μm were formed. The chamber was slowly cooled to room temperature (~24°C) and the vesicles were harvested in Eppendorf vials. These GUVs were used within 2 days.

Preparation of glass micropipettes

Capillary glass tubing (Fredrick & Dimmock, Millville, NJ) was drawn into a constant diameter shaft using a glass puller (David Kopf Instrument, Tujunga, CA) and fractured cleanly with a microforge (Stoelting, Wood Dale, IL) for inner diameters between 6 and 8 μm. The inner diameter was measured by inserting a probe pipette with a known diameter profile (characterized by scanning electron microscopy). The pipette was then coated with 1 vol% solution of SurfaSil in chloroform.

Methods

Micropipette aspiration

A chamber was constructed consisting of two parallel SurfaSil-coated glass coverslips, separated by spacers of ~2-mm thickness and ~1.5 cm apart and sealed with vacuum grease. To allow easy access of the micropipette, the chamber was left open on two sides. The chamber was placed on the microscope stage of an inverted Nikon Diaphot 300 microscope (Nikon, Melville, NY) equipped with a 40× Long Working Distance Hoffman modulation contrast objective (Modulation Optics, Greenvale, NY), a high-resolution charge-coupled device camera (Dage MTI, Michigan City, IN), and a Super VHS recorder (Sony SVO-9500MD, Tokyo, Japan). The chamber was filled with a glucose solution in water or water/ethanol and GUVs were added at room temperature (~24°C). The concentration of ethanol in water ranged from 0 to 25% (vol/vol). The concentration of the glucose was adjusted to optimize the initial projection length and ranged from 92 to 105 mM. A micropipette was filled with the same solution as found in the chamber plus 0.2 wt% bovine serum albumin and connected to a micromanipulator (model MHW-3, Narishige, Tokyo, Japan) to control the pipette's position in the chamber. The micropipette was connected to a water chamber through a length of thin water-filled tubing. Suction was created by adjusting the height of the chamber using a slider and micrometer (Velmex, Bloomfield, NY) below the height of the micropipette tip and used to aspirate individual GUVs into the micropipette (Fig. 2). The aspiration pressure, ΔP, was measured by an attached Acu-Rite ENC 150 linear encoder (Acu-Rite, Jamestown, NY) connected to a digital readout box and video overlay box (Polvision, Perth, Australia). Aspiration of GUVs and overlaid time and pressure data were recorded to S-VHS videotape. Digitized pictures with a resolution of 300 nm/pixel were taken at different pressures to determine the geometrical deformation of the vesicles. Image analysis was performed using the ATI Multimedia Center TV program (ATI Technologies, Markham, Ontario, Canada). Data treatment was performed as described below.

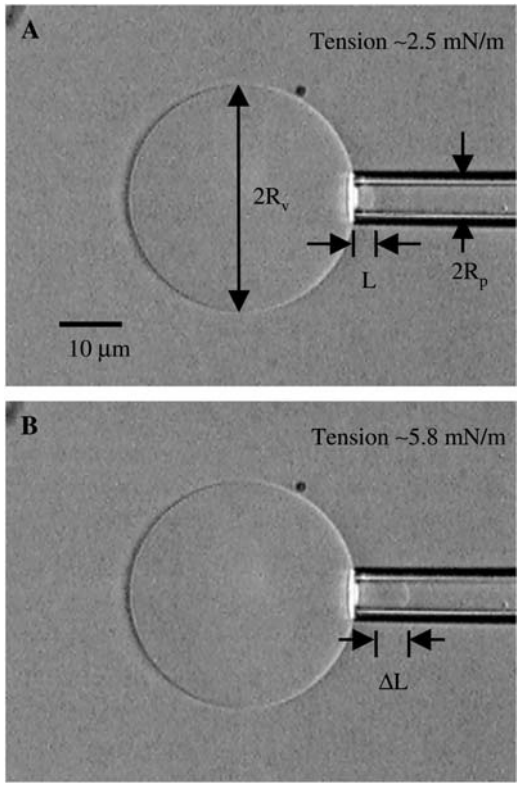

FIGURE 2 Video micrograph of a giant unilamellar vesicle (80 mol% DPPC/20 mol% ergosterol) in 10 vol% ethanol during aspiration demonstrating the increase in projection length, L, as the membrane tension, τ, is adjusted from (*A*) 2.5 mN/m to (*B*) 5.8 mN/m.

MPA calculations

The area compressibility (or elastic) modulus of each GUV aspirated was calculated using the method developed by Evans and others (reviewed in Evans and Needham (59)). The suction pressure, ΔP, applied to the vesicle produces a uniform membrane tension, τ, which can be described as shown below by a relation between the pipette radius, R_p, and the vesicle radius, R_v.

$$\tau = \frac{\Delta P R_p}{2\left(1 - \frac{R_p}{R_v}\right)}. \quad (1)$$

Fig. 2 shows that as suction pressure inside the pipette builds (and the membrane tension increases), the projection length of the GUV inside the pipette, L, increases in length. The change in the projection length, ΔL, can directly give the overall area increase of the membrane, ΔA, by subtracting the membrane area at the initial tension, A_0, from the membrane area, A, at each interval measured. Assuming the volume of the vesicle is fixed, the apparent area strain, α, can be calculated using the following approximation:

$$\alpha = \frac{\Delta A}{A_0} \approx \frac{1}{2}\left\{\left(\frac{R_p}{R_v}\right)^2 - \left(\frac{R_p}{R_v}\right)^3\right\}\frac{\Delta L}{R_p}. \quad (2)$$

The area compressibility modulus (K_a) was calculated using measurements taken in the high-tension range (>0.5 mN/m) of the vesicle membrane. In this regime, increases in α are almost entirely due to an increase in the area per molecule of the membrane. The contribution to α by damping of thermal undulations can be estimated and is quite small for K_a values above 350 mN/m, but not negligible for lower values; therefore, our reported K_a values below 350 mN/m should be viewed as apparent K_a values. After a preliminary increase in suction pressure to remove any excess membrane folds, tubes, or vesicles, and to check the vesicle for reversibility of projection length, the suction pressure inside the pipette was increased in steps. At each step, the membrane was allowed to come to equilibrium before measurements were taken. The τ of each successive step was plotted against its calculated α. This plot was linear for most of the data (see Fig. 3) and its slope is equal to the area compressibility modulus, K_a (i.e., $K_a \sim \tau/\alpha$).

RESULTS AND DISCUSSION

Tables 2 and 3 summarize the impact of membrane sterol content and ethanol solution concentration on the mechanical behavior and visual appearance of giant unilamellar DPPC vesicles at 24°C, studied here. In the majority of the conditions shown, these vesicles appeared spherical and behaved elastically upon micropipette aspiration. For each of these conditions, the area compressiblity modulus was measured and is noted in the tables. For some vesicles, plots of the tension versus apparent area strain exhibited a discontinuity at a critical tension, resulting in two distinct slopes. This behavior is noted with an asterisk and both slopes are reported. For vesicles that did not behave as reasonably cohesive fluids when aspirated, identification of physical characteristics was carried out by visual inspection. These vesicles were labeled as ''Gel'', ''Interdigitated'', ''Gel-like'', or ''Fragile''.

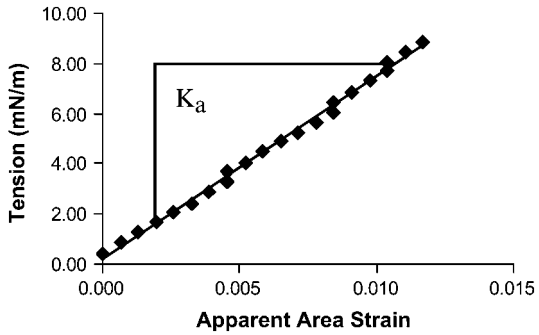

FIGURE 3 Measurements of tension, τ, are plotted versus apparent area strain, α, for an aspirated GUV (75 mol% DPPC/ 25 mol% ergosterol).

TABLE 2 Area compressibility modulus, K_a, values for membranes of giant unilamellar vesicles of different DPPC/ cholesterol (CHOL) compositions in environments of varying ethanol concentrations

Ethanol concentration (vol%)	K_a (mN/m)	No. of vesicles	Second linear slope (mN/m)
Pure DPPC			
0	Gel		
5	Gel/interdigitated		
10	Interdigitated		
12	Interdigitated		
95 mol% DPPC/5 mol% CHOL			
0	Gel		
12	Interdigitated		
90 mol% DPPC/10 mol% CHOL			
0	407.6 ± 130.2	7	
10	Gel-like		
85 mol% DPPC/15 mol% CHOL			
0	348.0 ± 97.4	22	
5	267.4 ±124.3	9	
10	168.4 ± 47.8*	8	72.3 [1]
15	Interdigitated		
25	Interdigitated		
82 mol% DPPC/18 mol% CHOL			
0	1116.2 ± 187.1	12	
80 mol% DPPC/20 mol% CHOL			
0	1155.1 ± 276.4	10	
5	919.3 ± 168.9	17	
10	666.6 ± 58.4	10	
15	482.6 ± 190.2*	7	79.2 ± 42.5 [5]
20	Fragile/interdigitated		
75 mol% DPPC/25 mol% CHOL			
0	1149.8 ± 119.9	11	
10	1089.1 ± 178.8	10	
15	714.7 ± 193.8	9	
20	781.8 ± 241.6*	9	204.8 ± 181.8 [4]
25	Interdigitated		
70 mol% DPPC/30 mol% CHOL			
15	657.9 ± 123.0	10	
60 mol% DPPC/40 mol% CHOL			
0	1281.2 ± 140.8	21	
10	1120.4 ± 178.5	11	
20	1099.7 ± 168.6	8	
25	1054.2 ± 115.7	8	

Observation of a second linear slope is indicated by an asterisk. The numbers in brackets for these values represent the number of vesicles where this occurred.

TABLE 3 Area compressibility modulus, K_a, values for membranes of giant unilamellar vesicles of different DPPC/ergosterol (ERG) compositions in environments of varying ethanol concentrations

Ethanol concentration (vol%)	K_a (mN/m)	No. of vesicles	Second linear slope (mN/m)
90 mol% DPPC/10 mol% ERG			
0	245.7 ± 35.1	10	
5	216.7 ± 30.3	10	
10	Gel-like		
15	Interdigitated		
85 mol% DPPC/15 mol% ERG			
0	344.1 ± 60.6	12	
82 mol% DPPC/18 mol% ERG			
0	780.7 ± 142.3	10	
80 mol% DPPC/20 mol% ERG			
0	746.0 ± 258.7*	11	238.3 ± 18.7 [7]
5	775.1 ± 151.2*	8	403.1 ± 125.9 [4]
10	221.4 ± 49.3*	12	81.1 ± 46.4 [2]
15	Gel-like		
20	Interdigitated		
75 mol% DPPC/25 mol% ERG			
0	691.4 ± 125.3	10	
5	908.2 ± 125.9	9	
10	831.1 ± 237.5	12	
15	Gel-like		
20	Interdigitated		
60 mol% DPPC/40 mol% ERG			
0	1162.5 ± 299.8	7	
5	1142.0 ± 204.2	10	
10	1111.2 ± 244.6	9	
15	747.6 ± 109.8	9	
20	879.2 ± 123.7	10	
25	Fragile		

Observation of a second linear slope is indicated by an asterisk. The numbers in brackets for these values represent the number of vesicles where this occurred.

To easily identify trends in mechanical and morphological behavior and propose possible ''phase diagrams,'' in Fig. 4, *A* and *B*, we have created ''elasticity diagrams'', i.e., placing our findings at their coordinates for mol% sterol and vol% ethanol. We have shaded in regions where the K_a values are so close in magnitude as to be indistinguishable as indicated by a student's *t*-test. Each K_a value in Fig. 4 *A* that was found to be statistically indistinguishable from the K_a value at the same sterol and ethanol concentrations in Fig. 4 *B* is indicated by a box around the data point. Proposed phase and microstructural behavior and approximate phase boundaries in Fig. 4, *A* and *B*, will be discussed below.

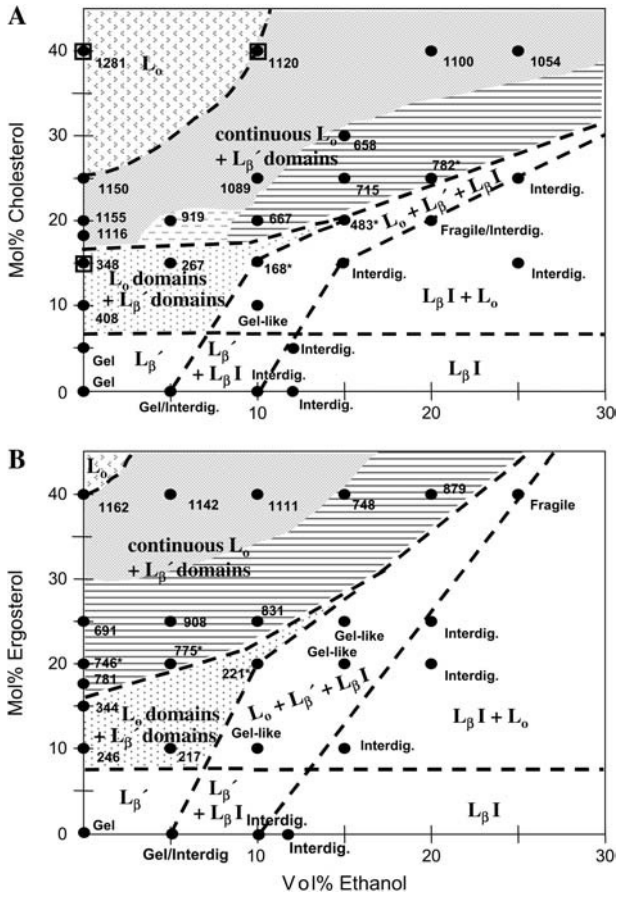

FIGURE 4 ''Elasticity/phase diagrams'' for DPPC/sterol membranes in water and water/ethanol solutions as characterized by MPA and visual observation. Membranes of GUVs contained (*A*) cholesterol and (*B*) ergosterol. The numbers correspond to area compressibility modulus (K_a) values. Values labeled with an asterisk displayed two slopes in tension versus area strain as listed in Tables 2 and 3. K_a was not determined for nonfluid vesicles, rather their mechanical behavior was identified as Gel, Gel-like, Interdig., and Fragile. We have shaded in regions where the K_a values are so close in magnitude as to be indistinguishable as indicated by a Student's *t*-test (two-tailed test table, $p = 0.05$) (exceptions are listed below). Each K_a value in panel *A* that was found to be significantly the same as the K_a value at the same sterol and ethanol concentrations in panel *B* is indicated by a box around the data point. The phases are labeled as follows: L_β', tilted gel phase; L_o, untilted liquid-ordered phase (an analogous ''L_o-like'' phase in the case of ergosterol); L_βI, interdigitated gel phase. Boundaries between regions are suggested based on the groupings of area compressibility moduli and general mechanical behavior as discussed in the text. In the striped shaded region, we postulate that the L_o phase is less condensed in comparison to L_o phase in the shaded gray region as indicated by a comparison of K_a values. Exceptions to statistical groupings of K_a values are: in panel *A*, 1155 was found not to be statistically different from 1281, 267 was found to be statistically different from 408; in panel *B*, 691 and 748 were found to be statistically different from 908 and 879, 1162 was not found to be statically different from 908.

DPPC/sterol vesicles in 0 vol% ethanol solution: mechanical behavior and visual appearance in relation to intermolecular interactions and phase behavior

For comparison to DPPC vesicles containing ergosterol and cholesterol, we first examined pure DPPC vesicles that are known to be in the L_β' phase. Pure DPPC GUVs displayed a distribution of morphologies but were mainly oblong (Fig. 5 *A*), with a smaller number of GUVs appearing spherical or ruffled (not shown). As expected for the rigid L_β' phase

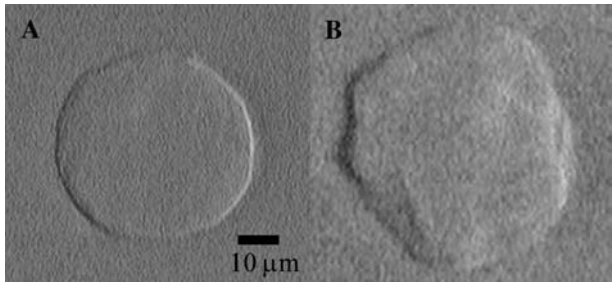

FIGURE 5 Video micrographs showing (*A*) pure DPPC oblong vesicle in the L_{β}' phase and (*B*) vesicle composed of 85 mol% DPPC/15 mol% cholesterol in 15 vol% ethanol exemplifying the highly ruffled visual appearance associated with interdigitation.

(a tilted gel phase) of DPPC, the surfaces of the GUVs appeared rigid and did not appear to thermally fluctuate at room temperature. Application of suction resulted in slow growth of the projection and the projection length did not decrease if the suction was decreased. If the GUV was ejected out of the pipette, the projection remained. We did not measure K_a for GUVs of pure DPPC and 95 mol% DPPC/5 mol% cholesterol that displayed these characteristics that are peculiar to crystalline bilayer phases of long-range lateral order (for example, see Fig. 6 and Evans and Needham (59)). Instead, in Tables 2 and 3 and Fig. 4, *A* and *B*, we label this behavior as Gel (L_{β}'). In Fig. 4, *A* and *B*, we assigned L_{β}' phase to the region in the bottom left corners where Gel behavior was observed.

Qualitatively, our results for the mechanical behavior and appearance of DPPC GUVs with increasing cholesterol concentration agree with the K_a measurements that exist for DMPC GUVs containing cholesterol (12.5, 33, and 50 mol%) at similar temperatures with respect to the main transition temperature (60). We made the same two observations when we added a small amount of cholesterol (~10 mol%): this percentage fluidized the lipid bilayer (compared to its pure state) and the K_a measured was low (~400 mN/m); see Table 2 and Fig. 4 *A*. Specifically, at low cholesterol (10–15 mol%), DPPC GUVs were uniformly spherical except for visible thermal fluctuations. When aspirated into the micropipette, these GUVs behaved as liquids with no surface shear rigidity. Tension versus apparent area expansion behavior was linear and reversible and the slope yielded relatively low average K_a values (~350–400 mN/m). The ''fluid'' nature and low K_a values support experimental evidence that at ~10 mol% cholesterol, submicron-scale domains of the L_{β}' gel phase lipid coexist with submicron-scale liquid-ordered (L_o) domains (36,60–65). The larger intermolecular spacing in the boundary regions between domains (compared to the intermolecular spacing in the bulk L_{β}' phase) and the lack of long-range order could account for the observed mechanical behavior. Therefore, at a concentration between 5 and 10 mol% cholesterol, we denote an approximate phase boundary between the L_{β}' phase and coexisting L_o domains + L_{β}' domains in Fig. 4 *A*.

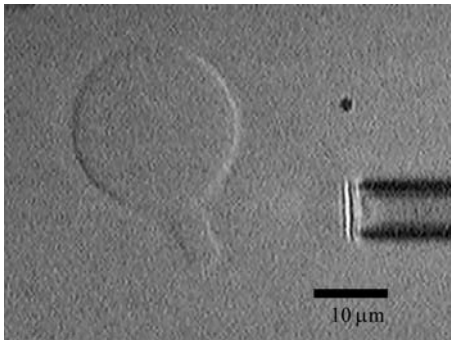

FIGURE 6 Video micrograph of a GUV (90 mol% DPPC/10 mol% cholesterol) in 10 vol% ethanol after being ejected from a pipette immediately after aspiration. The still visible projection is a clear indication of ''Gel-like'' bilayer properties. Gel vesicles also exhibit this behavior.

It is clear from other studies that a substantial change in cohesiveness and overall structure occurs in saturated PC membranes between ~10 and ~25 mol% cholesterol (60,61,66). The nature of the transition in area compressibility modulus (smooth versus abrupt) may reveal information about the overall microstructure and thermodynamics in this coexistence region, but it was unknown until this study. We find that there is a clear discontinuity in the magnitude of K_a between 15 and 18 mol% cholesterol and its value more than doubles from ~350 to ~1100 mN/m; see Table 2 and Fig. 4 *A*. Such a dramatic increase suggests that the area fraction of the cohesive L_o phase domains has increased just enough to form a continuous network. In support of this scenario, freeze fracture imaging by Lentz et al. (61) revealed that the membrane of DPPC multilamellar vesicles incorporating 24 mol% cholesterol near room temperature contained a planar network, ~100-nm wide, ''higher'' than the surrounding lipid, indicating a continuous network of the untilted L_o phase surrounding domains of the tilted L_{β}' phase. This morphology is reported to arise at ~20 mol% cholesterol, in close agreement with the concentration at which we detect the massive increase in K_a. Based on our results, at a concentration between 15 and 18 mol% cholesterol, in Fig. 4 *A*, we denote an approximate phase boundary between coexisting L_o domains + L_{β}' domains and continuous L_o + L_{β}' domains.

Experimentally, no evidence of L_{β}' phase lipid exists at >25 mol% cholesterol (62,67–69) and presumably the membrane contains only L_o phase. Therefore, at a concentration of ~25 mol% cholesterol, we denote a phase boundary between continuous L_o + L_{β}' domains and L_o phase in Fig. 4 *A*. The DPPC vesicles continued to act as liquids as the concentration of cholesterol was increased to 40 mol%. At 40 mol% cholesterol, K_a had increased to 1281 mN/m compared to 1150 mN/m at 25 mol% cholesterol, a small but statistically significant rise; see Table 2 and Fig. 4 *A*.

By comparing the mechanical behavior and visual appearance of DPPC GUVs containing cholesterol (Table

2; Fig. 4 *A*) with DPPC GUVs containing ergosterol (Table 3; Fig. 4 *B*), a general similarity in the effect of these sterols on the cohesive behavior is noted. Inclusion of 10 mol% ergosterol or cholesterol fluidized the DPPC vesicles and aspiration revealed a low K_a value ~300 mN/m. In addition for both sterols, a sharp increase in K_a of DPPC vesicles occurs between 15 and 18 mol% sterol. At 40 mol% sterol, the K_a values were statistically indistinguishable for DPPC vesicles containing cholesterol or ergosterol. The strikingly similar impact of these two sterols on the general mechanical behavior of the DPPC lipid bilayer is an indication that they are causing very similar changes in phase behavior and microstructure. In the case of cholesterol, it is fairly well established that the phase behavior is a result of the formation of L_o phase, which increases in area fraction as the cholesterol content increases. Although it has not been established yet, whether the L_o phase exists in lipid bilayers containing ergosterol or other sterols, we hypothesize that, in the case of ergosterol, a phase exists that can nominally be called ''L_o-like''. Like the L_o phase, associated with cholesterol, our results show that this L_o-like phase imparts a greatly increased lateral fluidity in comparison to the $L_{\beta'}$ phase and an increased stiffness as the sterol content is increased, while maintaining fluidity. Differences exist in the magnitude of the K_a values, indicating that ergosterol may induce a looser packing of the bilayer in comparison to cholesterol as will be discussed in the paragraph below. We place the phase boundaries between the $L_{\beta'}$ phase, $L_{\beta'}$ domains + L_o domains, and continuous L_o + $L_{\beta'}$ domains at roughly the same place for both ergosterol- and cholesterol-containing DPPC membranes (Fig. 4, *A* and *B*). Previous studies have not conclusively shown the ergosterol concentration at which the $L_{\beta'}$ phase is no longer present. We did not place the transition to pure L_o phase at ~25 mol%, the known transition for cholesterol, but instead place it at ~40 mol%. Here, the K_a values in Fig. 4, *A* and *B*, are indistinguishable and the phase is pure L_o for DPPC vesicles containing cholesterol.

Interestingly, a distinct decrease in the slope of τ vs. α occurred above a critical tension (Fig. 7) for some ergosterol-containing GUVs that are approximately on the phase boundary between continuous L_o + $L_{\beta'}$ domains and L_o domains + $L_{\beta'}$ domains (Fig. 4 *B*, points with *asterisks*). We believe the change in slope corresponded to a rearrangement of the continuous L_o network caused by aspiration, such that for a portion of the membrane, the network was no longer continuous. Similar, although more erratic, changes in slope were observed previously (51) for membranes containing coexisting gel phase network and intervening fluid phase and were attributed to a similar phenomena. The first slopes (746 and 775 mN/m), corresponds to stretching of the continuous phase and we believe, based on the range of second values (~200–400 mN/m), that the second slopes correspond to stretching of regions where the L_o phase is not continuous.

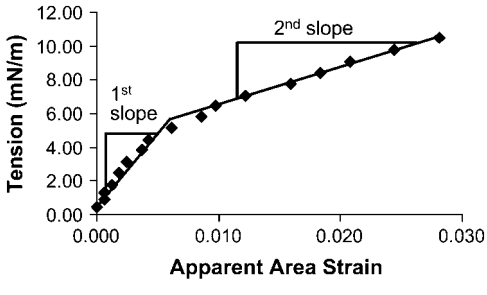

FIGURE 7 Tension-strain plot of a 80 mol% DPPC/20 mol% ergosterol vesicle. At a tension of ~6 mN/m, the transition between the two slopes becomes apparent.

Our studies indicate that ergosterol may be more disruptive of long-range cohesive packing of the $L_{\beta'}$ phase than cholesterol at very low concentrations (10 mol%) as indicated by the reasonably small, but significant, difference in average K_a values of ~400 mN/m (cholesterol) and ~250 mN/m (ergosterol). Ergosterol also seems to be less efficient at restoring long-range cohesive packing to this fluidized bilayer. When the transition to a more cohesive bilayer occurred between 15 and 18 mol% sterol, the area compressibility moduli were ~750 and ~1100 mN/m for ergosterol and cholesterol, respectively. This indicates that the intermolecular spacing in the continuous L_o phase was larger (i.e., less condensed with lower van der Waals interactions) for the membrane containing ergosterol in comparison to cholesterol. We indicate this less condensed continuous L_o phase by the striped shading in Fig. 4 *B*. Very little data exist concerning the differential behavior of ergosterol and cholesterol at concentrations below 25 mol% with respect to long-range order or cohesiveness of DPPC at room temperature. In support of our results, DPH mean fluorescence lifetime showed an initial decrease (from 0 to 10 mol%) for both cholesterol and ergosterol, attributed to possible increased water penetration in the bilayer due to the fluidization of the gel membrane (66). The magnitude of the decrease was significantly larger for ergosterol in comparison to cholesterol. The mean lifetimes showed an increase at 20 mol% sterol, attributed to a decrease in water penetration as the bilayer became more cohesive. At 20 mol%, the mean lifetime was less for bilayers containing ergosterol in comparison to cholesterol. The differential behavior of ergosterol and cholesterol with respect to restoring membrane cohesiveness in saturated lipids at concentrations near ~20 mol% cholesterol bears similarity to the behavior observed in unsaturated PC lipids. A handful of studies indicate that both ergosterol and cholesterol increase membrane density in unsaturated PC lipids, however the effect of ergosterol plateaus at ~20 mol%, whereas cholesterol further condenses the bilayer up to ~50 mol% (13,66,70). In the case of the interaction of ergosterol with unsaturated PC lipids, it has been hypothesized that its more bulky alkyl chain (in comparison to cholesterol) does not allow very close association of the two species.

At 40 mol% sterol the K_a values of DPPC membranes containing cholesterol and ergosterol are statistically the same, ~1280 and ~1160 mN/m, respectively. These data indicate that the two sterols are condensing the bilayer to a similar degree at 40 mol%, i.e., the bulky side chain of ergosterol is no longer preventing close interaction between the sterol group and lipid side chains in the L_o phase. Our results at this higher sterol percentage agree most closely with an NMR study that observed the degree of order in the entire chain of a saturated PC lipid (DMPC) at 30 mol% sterol (13). In comparing cholesterol and ergosterol with a related sterol, lanosterol, these investigators found that ergosterol and cholesterol induced similar order on the alkyl chains—indicating similar intermolecular distances (although they found that ergosterol ordered the bilayer slightly more than cholesterol). Additionally, Endress et al. performed micropipette aspiration on DPPC GUVs containing 40 mol% ergosterol and 40 mol% cholesterol and found that they had nearly identical lysis tension values, an indication of similar cohesive properties (71). However, the K_a value obtained by Endress et al. (71) for DPPC GUVs containing 40 mol% cholesterol is much lower (740 mN/m) than any of our measurements for DPPC GUVs containing 40 mol% cholesterol including GUVs exposed to 25 mol% ethanol.

DPPC/sterol vesicles in 5–25 vol% ethanol solution: mechanical behavior and visual appearance in relation to intermolecular interactions and phase behavior

For DPPC GUVs at most sterol concentrations discussed in the previous section, we then examined their mechanical and morphological behavior in ethanol solutions of increasing concentration, in steps of 5 vol%. Generally, there was a significant lowering in K_a, or change in general mechanical behavior, after addition of between 10 and 15 vol% ethanol. To understand these changes in terms of phase and microstructure, in Fig. 4, *A* and *B*, we grouped average K_a values together, by using the same shading, when they belonged to the same population (by *t*-test). For nonfluid vesicles we grouped by similar mechanical behavior and appearance (Gel, Gel-like, Interdigitated). The assignment of phase and microstructural behavior to these groups of K_a values in Fig. 4, *A* and *B*, is consistent with the previous section, e.g., the groupings with K_a values between 650 and 900 mN/m are ''looser packed'' continuous $L_o + L_\beta'$ domains. Thus, as it can be seen in Fig. 4, *A* and *B*, the lowering of K_a by ethanol represents phase or microstructural changes. For example, for DPPC GUVs containing 25 mol% cholesterol, addition of 15 vol% ethanol lowers K_a from 1150 to 715 mN/m representing a transition from continuous $L_o + L_\beta'$ domains (s*haded gray*) to the looser packed continuous $L_o + L_\beta'$ domains (*striped*).

We do not believe that the mechanism for the lowering of K_a, for any of the vesicles containing only L_o phase or the more tightly packed continuous L_o phase, involved interdigitation or even partial chain interdigitation. Similarly, we believe that all GUVs that displayed only one K_a value, above 650 mN/m, did not contain interdigitated lipid. The evidence for these assertions is a previous study (25) that showed an absence of any interdigitation in DPPC bilayers with a cholesterol content of 20 mol% in an ethanol concentration of ~10 vol%. Under the same conditions, we measured K_a values of 667 mN/m, reduced from 1155 mN/m in the absence of ethanol. It could be argued that the chains themselves were partially interdigitating. However, in a number of studies, it has been shown that ethanol does not induce partial chain interdigitation of ordered lipid phases. Rather at a threshold ethanol concentration, an area fraction of the bilayer becomes completely interdigitated (i.e., coexistence of interdigitated and noninterdigitated phases) and the area fraction of interdigitated phase increases steadily as the ethanol concentration is raised (20,72,73). Because of this absence of L_βI phase, we have assigned the entire top left corners of Fig. 4, *A* and *B*, as L_o or continuous $L_o + L_\beta'$ domains.

Interestingly, a large decrease in K_a was noted as ethanol volume percentage was increased to 10 vol% for 20 mol% ergosterol GUVs. Here the K_a value dropped from ~750 mN/m below 10 vol%, to ~200 mN/m at 10 vol%. We believe this represents a transition from the coexistence of continuous L_o phase + L_β' domains (i.e., population with K_a values between ~650 and ~900 mN/m as discussed above) to coexisting L_o domains + L_β' domains (i.e., population with K_a values between ~200 and 400 mN/m) as indicated by the phase boundary on Fig. 4 *B*. We cannot rule out the possible appearance of a small amount of interdigitated lipid as well; however, its presence is not necessary to explain the result.

Overall, this trend of decreasing area compressibility modulus suggests that ethanol is disrupting intermolecular attractive interactions within the membrane. Sterols interact with saturated gel phase lipids mainly by attractive van der Waals interactions (74), and possibly by hydrogen bonding and/or water bridge formation between the lipid headgroups and the alcohol groups on the sterols (75). Ethanol, which adsorbs into the headgroup near the upper tail region (16,76), will increase the polarity of this region. This increased polarity makes interaction in the upper tail region with water more favorable, resulting in increased intermolecular spacing and thus decreased attractive interactions (decrease in K_a) as we have observed in previous work involving unsaturated lipid bilayers (44,45). Moreover, ethanol can competitively hydrogen bond with lipid headgroups (18,21), adding to the disruption of sterol-lipid interactions. As the ethanol causes the interaction between sterol and DPPC to become weaker, the spacing between them increases (observed by us as a decrease in K_a of vesicles containing L_o phase) and the sterol-DPPC interactions become of similar magnitude to the DPPC-DPPC interactions. The latter should result in

a decrease in the area fraction of L_o phase. For example, at 20 mol% ergosterol, we observe an abrupt decrease in K_a between 5 and 10 vol% ethanol, which we attribute to a decrease in the area fraction of L_o phase; i.e., a transition from continuous L_o phase + $L_{\beta'}$ domains to coexisting L_o domains + $L_{\beta'}$ domains.

Above a threshold ethanol concentration for each sterol condition, the vesicles appearance changed dramatically. This is noted by the label, ''Interdigitated'' in Tables 2 and 3 and Fig. 4, *A* and *B*. In these cases, the giant vesicles uniformly did not have a rounded appearance. Instead, they appeared multifaceted or deeply ruffled (see Fig. 5 *B*). By comparison to a previous study (25), we found that DPPC vesicles known to contain a large percentage of L_{β}I phase, 0 or 5 mol% cholesterol in 12 vol% ethanol, also appeared multifaceted or deeply ruffled. The alcohol concentration where we noted this interdigitated vesicle morphology depended upon the sterol and its concentration. As the sterol concentration increased, more ethanol was required for the vesicles to change their appearance, and the transition occurred at a higher ethanol concentration for cholesterol-containing vesicles in comparison to ergosterol-containing vesicles. As L_{β}I phase area fraction increases, the cholesterol content should become enriched in the remaining L_o phase. Therefore, interdigitation resistant L_o phase may persist even for vesicles that appear to be interdigitated by visual inspection. Based upon our observations, in Fig. 4, *A* and *B*, the bottom right corners above sterol contents $>\sim$7 mol% was assigned as L_{β}I + L_o phases and below $\sim$7 mol% sterol as L_{β}I. Fragile vesicles also occurred within this region. Specifically, for two conditions, we observed vesicles that were so fragile (lysed at a low tension), that their behavior could not be characterized by MPA. These vesicles, labeled as ''Fragile'', appeared spherical and displayed surface fluctuations. The behavior of these vesicles may represent an occasional metastable lipid organizational state before interdigitation.

Now we will discuss the diagonal regions in Fig. 4, *A* and *B*, labeled as L_o + $L_{\beta'}$ + L_{β}I. In this region, L_o, $L_{\beta'}$, and L_{β}I phases coexist. This assignment is consistent with the phases present on the left boundary (coexisting L_o and $L_{\beta'}$ phases) and right boundary (coexisting L_{β}I and L_o phases) and the necessity for the existence of an intervening three-phase region. For DPPC GUVs containing cholesterol, this region was fairly narrow with a width of $\sim$5 vol% ethanol, between the observation of round fluid vesicles and severely ruffled vesicles, making it difficult to characterize the behavior of vesicles within the region at multiple cholesterol and ethanol concentrations. However, we were able to characterize one point, at 10 mol% cholesterol, 10 mol% ethanol. Previously, Komatsu and Rowe (25) found that an intermediate area fraction of L_{β}I existed under that condition. For DPPC GUVs containing ergosterol, the region was wider (5–10 vol%) and we were able to characterize three points. All GUVs within this region behaved similarly and are labeled as ''Gel-like'' in Tables 2 and 3 and Fig. 4, *A* and *B*. By micropipette aspiration, these GUVs behaved similarly to pure DPPC GUVs in 0 vol% ethanol; i.e., they displayed surface rigidity throughout aspiration. In particular, upon application of suction, the projection grew slowly. Upon reduction of tension, the projection remained. If expelled from the pipette entirely, the GUV would float away from the pipette with its projection still intact (see Fig. 6). Interestingly, before aspiration, these GUVs appeared spherical by interference contrast microscopy and displayed some surface thermal fluctuation. The assignment of the coexisting L_o, $L_{\beta'}$, and L_{β}I phases is consistent with the observed mechanical behavior, i.e., gel-like behavior upon aspiration as would be expected for GUVs containing the ordered crystalline L_{β}I phase, but generally round in shape and displaying a small degree of thermal fluctuation as expected for fluidized GUVs containing domains of $L_{\beta'}$ phase + L_o phase. On the left boundary of this region, GUVs occasionally displayed two distinct slopes of τ vs. α (points with *asterisks*). Generally, the second slope, when present, was $\sim$75 mN/m. This second slope may actually represent a plastic transition where the suction pressure is inducing interdigitation in a small area fraction of the bilayer. In the future, we plan to test for reversibility of the second slope; i.e., a lack of reversibility would signal a plastic transition. The change in slope generally occurred above 4.5 mN/m and reversibility was only checked carefully for tensions below $\sim$5 mN/m during a prestretch.

It is known that the addition of cholesterol to saturated gel phase PC lipid bilayers increases headgroup spacing, thus relieving headgroup crowding present in pure $L_{\beta'}$ phase PC bilayers (25). Ethanol, on the other hand, increases headgroup volume when added to pure saturated gel phase PC bilayers through adsorption into the headgroup region (21,77). Subsequent ethanol-induced interdigitation in pure gel phase bilayers results in increased headgroup spacing needed for the ethanol-associated headgroup. Therefore, it appears paradoxical that ethanol can induce interdigitation in DPPC membranes containing large amounts of cholesterol (e.g., 25 mol% cholesterol) where there is plenty of space for the headgroup. Our results indicate that in the presence of ethanol, DPPC-sterol interactions are weakened and thus the number/frequency of interdigitation-prone DPPC-DPPC interactions is increased. DPPC membranes containing ergosterol interdigitated at lower ethanol concentration in comparison to membranes containing cholesterol, reflecting weaker ergosterol-DPPC interaction (i.e., lower K_a values). Also, we postulate that as the ethanol concentration is raised, there will always be a region of L_o domains + $L_{\beta'}$ domains between the region of continuous L_o + $L_{\beta'}$ domains and L_o + $L_{\beta'}$ + L_{β}I. However, as the sterol concentration increases, the region becomes very narrow and therefore, we did not happen to pick the correct conditions to observe it above 20 mol% sterol.

Significance with respect to cellular evolution and ethanol tolerance

Taken from the perspective of cellular evolution, we find that ergosterol is a better fluidizer at low concentrations (10–25 mol%) in comparison to cholesterol. Our results indicate that ergosterol is quite disruptive of long-range gel-phase lateral order at very low concentrations (~10 mol%) resulting in a fluid membrane with cohesiveness similar to an unsaturated PC bilayer. This cohesiveness is somewhat restored at ~18 mol%, but the membrane is still fluid and fairly pliable, as indicated by the relatively low K_a value. This supports a previous postulation that the alkylation in ergosterol's side chain has been chosen by yeast during sterol evolution for enhancing membrane disorder as an alternative to synthesis of unsaturated fatty acids (1). In theory, the ergosterol concentration of a yeast's plasma membrane can be tuned between ~10 and ~25 mol% to control the overall fluidity and cohesiveness of the bilayer without ever attaining an extremely cohesive bilayer that strays too much from the properties of unsaturated PC lipids (i.e., the 18 mol% cholesterol bilayer). In addition, as discussed above, ergosterol does not increase chain ordering in unsaturated lipids at concentrations above ~25 mol% ergosterol, so there is no need for ergosterol levels to ever exceed 25 mol% in any organism. In higher eukaryotes, cholesterol is present in the plasma membrane at percentages close to 40 mol%. Therefore, it is interesting to compare the K_a values of DPPC bilayers containing cholesterol and ergosterol at these higher proportions. At this concentration, we find that cohesion in cholesterol- and ergosterol-containing membranes are similarly high. Thus, the reason why cholesterol was chosen over ergosterol in cellular evolution in higher eukaryotes is not clear based upon the area compressibility moduli measurements. Therefore, other parameters must be involved, such as high lipid and cholesterol diffusion (78) or possibly a related lack of gel-phase domains (71) in the case of saturated membranes containing high percentages of cholesterol.

Our data show that inclusion of cholesterol or ergosterol in DPPC membranes confers resistance to ethanol-induced interdigitation. At the extreme end, DPPC bilayers containing 40 mol% cholesterol appears to be so cohesive (K_a = 1281 mN/m) that 25 vol% ethanol only decreases K_a to 1054 mN/m and no interdigitation is observed. For DPPC bilayers of slightly less cohesiveness (K_a ~ 1150 mN/m), ~15 vol% ethanol is required to decrease the cohesiveness significantly (K_a ~ 450–800 mN/m) followed by clear signs of interdigitation at ~20 vol% ethanol. Finally, for bilayers containing ergosterol in the physiological upper concentration range for lower eukaryotes (~18–25 mol%), the bilayer is cohesive enough (K_a ~ 800 mN/m), that clear signs of interdigitation only appear at ~15 vol% ethanol (compared to ~7 vol% for pure DPPC). These ergosterol data support the idea that ergosterol can enhance survivability for cells exposed to high concentrations of ethanol normally experienced during wine fermentation (i.e., <15 vol%) or industrial alcohol production by preventing interdigitation, through enhanced cohesiveness and increased headgroup spacing. For DPPC vesicles containing small amounts of sterol (10–15 mol%) with K_a values of ~300 mN/m, the presence of the sterol does seem to provide some protection against interdigitation as we detect a decreased percentage of interdigitation when sterol was incorporated into the membrane in the presence of 10 vol% ethanol, in comparison to pure DPPC in the presence of 10 vol% ethanol, in agreement with previous work (25). Potentially, the limited solubility of sterol in DPPC $L_{\beta'}$ phase domains offers some protection through increased headgroup spacing and the presence of L_o domains provides protection. However, our data suggest that the plasma membranes of yeast containing these lower concentrations of ergosterol (<18 mol%) will experience some degree of interdigitation initiating at an ethanol concentration of ~10 vol%. Previous studies with yeast under enological conditions have attributed ethanol tolerance to compositional changes that increase membrane fluidity, whereas others, in seemingly contradictory studies, have observed increased membrane fluidity simply upon introduction of ethanol to the cellular environment (31,79–83). It is clear from the phase diagrams in Fig. 4 how both of these observations might arise from experiments at various levels of ethanol and membrane ergosterol content. However, it is also clear that the appearance of interdigitated, $L_{\beta}I$, phase bilayer may be a major factor in disruption of alcoholic fermentation and may explain partially the appearance of disrupted ''stuck'' fermentations that typically occur between 12 and 16 vol% ethanol (37,38,81), a phenomenon that has yet to be implicated in previous studies.

CONCLUSIONS

The ''elasticity/phase'' diagrams (Fig. 4, *A* and *B*) summarize our main observations and conclusions: 1), DPPC membranes containing ergosterol and cholesterol exposed to ethanol solutions display similar overall mechanical and phase behavior; 2), there is an abrupt change in K_a value at ~18 mol% sterol, which we relate to a change in microstructure from coexisting $L_{\beta'}$ domains + L_o domains to coexisting continuous L_o + $L_{\beta'}$ domains; 3), the K_a values for ergosterol-containing membranes are generally lower than those for cholesterol-containing membranes at all alcohol concentrations (this is especially evident for sterol content ≥18 mol% and ≤25 mol% sterol, indicating larger intermolecular spacing and supporting the postulate that ergosterol serves as a replacement for unsaturated lipids in many lower eukaryotes); 4), a reduction in sterol content and increase in ethanol concentration decreases the bilayer K_a value through a decrease in lipid-sterol intermolecular attractions as required for induction of interdigitation; and 5), for sterol concentrations of 20–25 mol%, ethanol-induced

interdigitation is offset by ~7 and 10 vol% by ergosterol and cholesterol, respectively. For lower sterol concentrations (10–15 mol%), interdigitation is offset, but by <5 vol%. These data support the idea that sterols do enhance survivability for cells exposed to high concentrations of ethanol. Overall, for ''normal'' ergosterol contents (~10–25 mol%) interdigitation should become a major disruptive factor at ~12–16 vol% ethanol according to our ''phase diagram''. This concentration range corresponds well to ethanol concentrations at which fermentation activity is disrupted under enological conditions and a ''stuck'' fermentation occurs.

M.L.L. acknowledges the generous gift of Joe and Essie Smith for endowing part of this work. We acknowledge the helpful contributions of Hung Van Ly.

This work was funded primarily by the American Vineyard Foundation and the California Competitive Grant Program for Research in Viticulture and Enology. The Center for Polymeric Interfaces and Macromolecular Assemblies (grant NSF DMR 0213618), the Materials Research Institute at Lawrence Livermore National Laboratory (MI-03-117), and the Nanoscale Interdisciplinary Research Teams Program of the National Science Foundation (under award No. CHE 0210807) provided additional funding.

REFERENCES

1. Bloch, K. E. 1983. Sterol structure and membrane-function. *CRC Crit. Rev. Biochem.* 14:47–92.
2. Bloom, M., and O. G. Mouritsen. 1988. The evolution of membranes. *Can. J. Chem.* 66:706–712.
3. Bloom, M., E. Evans, and G. Mouritsen. 1991. Physical properties of the fluid lipid-bilayer component of cell membranes: a perspective. *Q. Rev. Biophys.* 24:293–397.
4. Brown, D. A., and E. London. 2000. Structure and function of sphingolipid- and cholesterol-rich membrane rafts. *J. Biol. Chem.* 275:17221–17224.
5. Yeagle, P. L. 1985. Cholesterol and the cell-membrane. *Biochim. Biophys. Acta.* 822:267–287.
6. McMullen, T. P. W., and R. N. McElhaney. 1996. Physical studies of cholesterol-phospholipid interactions. *Curr. Opin. Colloid Interface Sci.* 1:83–90.
7. Finegold, L. 1993. Cholesterol in Model Membranes. CRC Press, Boca Raton, FL.
8. Vereb, G., J. Szollosi, J. Matko, P. Nagy, T. Farkas, L. Vigh, L. Matyus, T. A. Waldmann, and S. Damjanovich. 2003. Dynamic, yet structured: the cell membrane three decades after the Singer-Nicolson model. *Proc. Natl. Acad. Sci. USA.* 100:8053–8058.
9. Simons, K., and E. Ikonen. 1997. Functional rafts in cell membranes. *Nature.* 387:569–572.
10. Bagnat, M., S. Keranen, A. Shevchenko, A. Shevchenko, and K. Simons. 2000. Lipid rafts function in biosynthetic delivery of proteins to the cell surface in yeast. *Proc. Natl. Acad. Sci. USA.* 97:3254–3259.
11. Rietveld, A., S. Neutz, K. Simons, and S. Eaton. 1999. Association of sterol- and glycosylphosphatidylinositol-linked proteins with Drosophila raft lipid microdomains. *J. Biol. Chem.* 274:12049–12054.
12. Chi, Z., and N. Arneborg. 2000. Saccharomyces cerevisiae strains with different degrees of ethanol tolerance exhibit different adaptive responses to produced ethanol. *J. Ind. Microbiol. Biotechnol.* 24:75–78.
13. Urbina, J. A., S. Pekerar, H. B. Le, J. Patterson, B. Montez, and E. Oldfield. 1995. Molecular order and dynamics of phosphatidylcholine bilayer-membranes in the presence of cholesterol, ergosterol and lanosterol: a comparative study using H-2-Nmr, C-13-Nmr and P-31-Nmr spectroscopy. *Biochim. Biophys. Acta.* 1238:163–176.
14. Arneborg, N., C. E. Hoy, and O. B. Jorgensen. 1995. The effect of ethanol and specific growth-rate on the lipid-content and composition of Saccharomyces cerevisiae grown anaerobically in a chemostat. *Yeast.* 11:953–959.
15. Bottema, C. D. K., R. J. Rodriguez, and L. W. Parks. 1985. Influence of sterol structure on yeast plasma membrane properties. *Biochim. Biophys. Acta.* 813:313–320.
16. Feller, S. E., C. A. Brown, D. T. Nizza, and K. Gawrisch. 2002. Nuclear Overhauser enhancement spectroscopy cross-relaxation rates and ethanol distribution across membranes. *Biophys. J.* 82:1396–1404.
17. Westh, P., and C. Trandum. 1999. Thermodynamics of alcohol-lipid bilayer interactions: application of a binding model. *Biochim. Biophys. Acta.* 1421:261–272.
18. Holte, L. L., and K. Gawrisch. 1997. Determining ethanol distribution in phospholipid multilayers with MAS-NOESY spectra. *Biochemistry.* 36:4669–4674.
19. Klemm, W. R., and H. J. Williams. 1996. Amphiphilic binding site of ethanol in reversed lipid micelles. *Alcohol.* 13:133–138.
20. Mou, J., J. Yang, C. Huang, and Z. Shao. 1994. Alcohol induces interdigitated domains in unilamellar phosphatidylcholine bilayers. *Biochemistry.* 33:9981–9985.
21. Barry, J. A., and K. Gawrisch. 1995. Effects of ethanol on lipid bilayers containing cholesterol, gangliosides, and sphingomyelin. *Biochemistry.* 34:8852–8860.
22. Jones, R. P. 1989. Biological principles for the effects of ethanol. *Enzyme Microb. Technol.* 11:130–153.
23. Löbbecke, L., and G. Cevc. 1995. Effects of short-chain alcohols on the phase behavior and interdigitation of phosphatidylcholine bilayer membranes. *Biochim. Biophys. Acta.* 1237:59–69.
24. Rowe, E. S. 1992. Effects of ethanol on membrane lipids. *In* Alcohol and Neurobiology: Receptors, Membranes, and Channels. R. R. Watson, editor. CRC Press, Boca Raton, FL. 239–267.
25. Komatsu, H., and E. S. Rowe. 1991. Effect of cholesterol on the ethanol-induced interdigitated gel phase in phosphatidylcholine: use of fluorophore pyrene-labeled phosphatidylcholine. *Biochemistry.* 30:2463–2470.
26. Ohki, K., K. Tamura, and I. Hatta. 1990. Ethanol induces interdigitated gel phase (L[beta]I) between lamellar gel phase (L[beta]′) and ripple phase (P[beta]′) in phosphatidylcholine membranes: a scanning density meter study. *Biochim. Biophys. Acta.* 1028:215–222.
27. Nambi, P., E. S. Rowe, and T. J. Mcintosh. 1988. Studies of the ethanol-induced interdigitated gel phase in phosphatidylcholines using the fluorophore 1,6-diphenyl-1,3,5-hexatriene. *Biochemistry.* 27:9175–9182.
28. Slater, J. L., and C. H. Huang. 1988. Interdigitated bilayer membranes. *Prog. Lipid Res.* 27:325–359.
29. Rowe, E. S. 1985. Thermodynamic reversibility of phase transitions. Specific effects of alcohols on phosphatidylcholines. *Biochim. Biophys. Acta.* 813:321–330.
30. Simon, S. A., and T. J. McIntosh. 1984. Interdigitated hydrocarbon chain packing causes the biphasic transition behavior in lipid/alcohol suspensions. *Biochim. Biophys. Acta.* 773:169–172.
31. Alexandre, H., J. P. Berlot, and C. Charpentier. 1994. Effect of ethanol on membrane fluidity of protoplasts from Saccharomyces cerevisiae and Kloeckera apiculata grown with or without ethanol, measured by fluorescence anisotropy. *Biotechnol. Tech.* 8:295–300.
32. Avdulov, N. A., S. V. Chochina, L. J. Draski, R. A. Deitrich, and W. G. Wood. 1995. Chronic ethanol-consumption alters effects of ethanol in-vitro on brain membrane-structure of high alcohol sensitivity and low alcohol sensitivity rats. *Alcohol. Clin. Exp. Res.* 19: 886–891.
33. Chin, J. H., and D. B. Goldstein. 1977. Effects of low concentrations of ethanol on the fluidity of spin labeled erythrocyte and brain membranes. *Mol. Pharmacol.* 13:435–441.

34. Ly, H. V., and M. L. Longo. 2004. Probing the interdigitated phase of a DPPC lipid bilayer by micropipette aspiration. *Macromol. Symp.* 219:97–122.

35. Pappayee, N., and A. K. Mishra. 2001. Evaluation of 1-naphthol as a convenient fluorescent probe for monitoring ethanol-induced interdigitation in lipid bilayer membrane. *Photochem. Photobiol.* 73:573–578.

36. Rosser, M. F. N., H. M. Lu, and P. Dea. 1999. Effects of alcohols on lipid bilayers with and without cholesterol: the dipalmitoylphosphatidylcholine system. *Biophys. Chem.* 81:33–44.

37. Bisson, L. F., and D. E. Block. 2002. Ethanol tolerance in *Saccharomyces. In* Biodiversity and Biotechnology of Wine Yeasts. M. Ciani, editor. Research Signpost, Kerala, India. 86–98.

38. Cramer, A. C., S. Vlassides, and D. E. Block. 2002. Kinetic model for nitrogen-limited wine fermentations. *Biotechnol. Bioeng.* 77:49–60.

39. Chi, Z., S. D. Kohlwein, and F. Paltauf. 1999. Role of phosphatidylinositol (PI) in ethanol production and ethanol tolerance by a high ethanol producing yeast. *J. Ind. Microbiol. Biotechnol.* 22:58–63.

40. Traverso-Rueda, S., and R. E. Kunkee. 1982. The role of sterols on growth and fermentation of wine yeasts under vinification conditions. *Dev. Ind. Microbiol.* 23:131–143.

41. Trandum, C., P. Westh, K. Jorgensen, and O. G. Mouritsen. 2000. A thermodynamic study of the effects of cholesterol on the interaction between liposomes and ethanol. *Biophys. J.* 78:2486–2492.

42. Lafon-Lafourcade, S., F. Larue, and P. Ribereau-Gayon. 1979. Evidence for the existence of survival factors as an explanation for some peculiarities of yeast growth especially in grape must of high sugar concentration. *Appl. Environ. Microbiol.* 38:1069–1073.

43. Johnson, D. A., N. M. Lee, R. Cooke, and H. H. Loh. 1979. Ethanol-induced fluidization of brain lipid bilayers: required presence of cholesterol in membranes for the expression of tolerance. *Mol. Pharmacol.* 15:739–746.

44. Ly, H. V., D. E. Block, and M. L. Longo. 2002. Interfacial tension effect of ethanol on lipid bilayer rigidity, stability, and area/molecule: a micropipet aspiration approach. *Langmuir.* 18:8988–8995.

45. Ly, H. V., and M. L. Longo. 2004. The influence of short-chain alcohols on interfacial tension, mechanical properties, area/molecule, and permeability of fluid lipid bilayers. *Biophys. J.* 87:1013–1033.

46. Needham, D., and D. V. Zhelev. 2000. Use of micropipet manipulation techniques to measure the properties of giant lipid vesicles. *In* Giant Vesicles. P. Walde, editor. John Wiley & Sons, Ltd., Brisbane, Australia. 103–147.

47. Needham, D., and D. V. Zhelev. 1996. The mechanochemistry of lipid vesicles examined by micropipet manipulation techniques. *In* Vesicles. M. Rosoff, editor. Marcel Dekker, New York, NY. 373–444.

48. Evans, E. A. 1989. Structure and deformation properties of red blood-cells: concepts and quantitative methods. *Methods Enzymol.* 173:3–35.

49. Kwok, R., and E. Evans. 1981. Thermoelasticity of large lecithin bilayer vesicles. *Biophys. J.* 35:637–652.

50. Discher, B. M., Y. Y. Won, D. S. Ege, J. C. M. Lee, F. S. Bates, D. E. Discher, and D. A. Hammer. 1999. Polymersomes: tough vesicles made from diblock copolymers. *Science.* 284:1143–1146.

51. Shoemaker, S. D., and T. K. Vanderlick. 2003. Material studies of lipid vesicles in the L-alpha and L-alpha-gel coexistence regimes. *Biophys. J.* 84:998–1009.

52. Longo, M. L., A. J. Waring, L. M. Gordon, and D. A. Hammer. 1998. Area expansion and permeation of phospholipid membrane bilayers by influenza fusion peptides and melittin. *Langmuir.* 14:2385–2395.

53. Zhelev, D. V., N. Stoicheva, P. Scherrer, and D. Needham. 2001. Interaction of synthetic HA2 influenza fusion peptide analog with model membranes. *Biophys. J.* 81:285–304.

54. Longo, M. L., A. J. Waring, and D. A. Hammer. 1997. Interaction of the influenza hemagglutinin fusion peptide with lipid bilayers: area expansion and permeation. *Biophys. J.* 73:1430–1439.

55. Needham, D., and D. V. Zhelev. 1995. Lysolipid exchange with lipid vesicle membranes. *Ann. Biomed. Eng.* 23:287–298.

56. Santore, M. M., D. E. Discher, Y. Y. Won, F. S. Bates, and D. A. Hammer. 2002. Effect of surfactant on unilamellar polymeric vesicles: altered membrane properties and stability in the limit of weak surfactant partitioning. *Langmuir.* 18:7299–7308.

57. Angelova, M. I., S. Soléau, P. Méléard, J. F. Faucon, and P. Bothorel. 1992. Preparation of giant vesicles by external AC fields. *Prog. Colloid Polym. Sci.* 89:127–131.

58. Israelachvili, J. 1992. Intermolecular & Surface Forces. Academic Press, San Diego, CA.

59. Evans, E., and D. Needham. 1987. Physical properties of surfactant bilayer-membranes: thermal transitions, elasticity, rigidity, cohesion, and colloidal interactions. *J. Phys. Chem.* 91:4219–4228.

60. Needham, D., T. J. Mcintosh, and E. Evans. 1988. Thermomechanical and transition properties of dimyristoylphosphatidylcholine cholesterol bilayers. *Biochemistry.* 27:4668–4673.

61. Lentz, B. R., D. A. Barrow, and M. Hoechli. 1980. Cholesterol-phosphatidylcholine interactions in multilamellar vesicles. *Biochemistry.* 19:1943–1954.

62. McMullen, T. P. W., and R. N. McElhaney. 1995. New aspects of the interaction of cholesterol with dipalmitoylphosphatidylcholine bilayers as revealed by high-sensitivity differential scanning calorimetry. *Biochim. Biophys. Acta.* 1234:90–98.

63. Huang, T. H., C. W. B. Lee, S. K. Das Gupta, A. Blume, and R. G. Griffin. 1993. A 13C and 2H nuclear magnetic resonance study of phosphatidylcholine/cholesterol interactions: characterization of liquid-gel phases. *Biochemistry.* 32:13277–13287.

64. Ipsen, J. H., G. Karlstrom, O. G. Mouritsen, H. Wennerstrom, and M. J. Zuckermann. 1987. Phase equilibria in the phosphatidylcholine-cholesterol system. *Biochim. Biophys. Acta.* 905:162–172.

65. Veatch, S. L., and S. L. Keller. 2003. Separation of liquid phases in giant vesicles of ternary mixtures of phospholipids and cholesterol. *Biophys. J.* 85:3074–3083.

66. Arora, A., H. Raghuraman, and A. Chattopadhyay. 2004. Influence of cholesterol and ergosterol on membrane dynamics: a fluorescence approach. *Biochem. Biophys. Res. Commun.* 318:920–926.

67. Estep, T. N., D. B. Mountcastle, R. L. Biltonen, and T. E. Thompson. 1978. Studies on anomalous thermotropic behavior of aqueous dispersions of dipalmitoylphosphatidylcholine-cholesterol mixtures. *Biochemistry.* 17:1984–1989.

68. Vist, M. R., and J. H. Davis. 1990. Phase equilibria of cholesterol dipalmitoylphosphatidylcholine mixtures deuterium NMR and differential scanning calorimetry. *Biochemistry.* 29:451–464.

69. McMullen, T. P. W., C. Vilcheze, R. N. Mcelhaney, and R. Bittman. 1995. Differential scanning calorimetric study of the effect of sterol side-chain length and structure on dipalmitoylphosphatidylcholine thermotropic phase-behavior. *Biophys. J.* 69:169–176.

70. Semer, R., and E. Gelerinter. 1979. Spin label study of the effects of sterols on egg lecithin bilayers. *Chem. Phys. Lipids.* 23:201–211.

71. Endress, E., S. Bayerl, K. Prechtel, C. Maier, R. Merkel, and T. M. Bayerl. 2002. The effect of cholesterol, lanosterol, and ergosterol on lecithin bilayer mechanical properties at molecular and microscopic dimensions: a solid-state NMR and micropipet study. *Langmuir.* 18:3293–3299.

72. Vierl, U., L. Lobbecke, N. Nagel, and G. Cevc. 1994. Solute effects on the colloidal and phase-behavior of lipid bilayer-membranes: ethanol-dipalmitoylphosphatidylcholine mixtures. *Biophys. J.* 67: 1067–1079.

73. Laggner, P., K. Lohner, R. Koynova, and B. Tenchov. 1991. The influence of low amounts of cholesterol on the interdigitated gel phase of hydrated dihexadecylphosphatidylcholine. *Chem. Phys. Lipids.* 60:153–161.

74. Vanderkooi, G. 1994. Computation of mixed phosphatidylcholine-cholesterol bilayer structures by energy minimization. *Biophys. J.* 66: 1457–1468.

75. Smondyrev, A. M., and M. L. Berkowitz. 2001. Molecular dynamics simulation of the structure of dimyristoylphosphatidylcholine

bilayers with cholesterol, ergosterol, and lanosterol. *Biophys. J.* 80: 1649–1658.

76. Chiou, J.-S., P. R. Krishna, H. Kamaya, and I. Ueda. 1992. Alcohols dehydrate lipid membranes: an infrared study on hydrogen bonding. *Biochim. Biophys. Acta.* 1110:225–233.
77. Nagel, N. E., G. Cevc, and S. Kirchner. 1992. The mechanism of the solute-induced chain interdigitation in phosphatidylcholine vesicles and characterization of the isothermal phase-transitions by means of dynamic light-scattering. *Biochim. Biophys. Acta.* 1111:263–269.
78. Endress, E., H. Heller, H. Casalta, M. F. Brown, and T. M. Bayerl. 2002. Anisotropic motion and molecular dynamics of cholesterol, lanosterol, and ergosterol in lecithin bilayers studied by quasi-elastic neutron scattering. *Biochemistry.* 41:13078–13086.
79. Thomas, D. S., J. A. Hossack, and A. H. Rose. 1978. Plasma-membrane lipid-composition and ethanol tolerance in Saccharomyces cerevisiae. *Arch. Microbiol.* 117:239–245.
80. Lloyd, D., S. Morrell, H. N. Carlsen, H. Degn, P. E. James, and C. C. Rowlands. 1993. Effects of growth with ethanol on fermentation and membrane fluidity of Saccharomyces cerevisiae. *Yeast.* 9:825–833.
81. Bisson, L. F. 1999. Stuck and sluggish fermentations. *Am. J. Enol. Vitic.* 50:107–119.
82. Jones, R. P., and P. F. Greenfield. 1987. Ethanol and the fluidity of the yeast plasma-membrane. *Yeast.* 3:223–232.
83. Agudo, L. D. 1992. lipid-content of Saccharomyces cerevisiae strains with different degrees of ethanol tolerance. *Appl. Microbiol. Biotechnol.* 37:647–651.